2011 IEEE/RSJ International Conference on
Intelligent Robots and Systems
September 25-30, 2011. San Francisco, CA, USA

Variable Radius Pulley Design Methodology for Pneumatic Artificial Muscle-based Antagonistic Actuation Systems

Dongjun Shin[1], Xiyang Yeh[2], and Oussama Khatib[1]
[1]*Artificial Intelligence Laboratory, Stanford University, Stanford, CA 94305, USA*
{*djshin, ok*}*@robotics.stanford.edu*
[2]*Mechanical Engineering, Stanford University, Stanford, CA 94305, USA*
xyyeh@stanford.edu

***Abstract*— There is a growing interest in utilizing pneumatic artificial muscles (PAMs) as actuators for human-friendly robots. However, several performance drawbacks prevent the widespread use of PAMs. Although many approaches have been proposed to overcome the low control bandwidth of PAMs, some limitations of PAMs such as restricted workspace and torque capacity remain to be addressed. This paper analyzes the limitations of conventional circular pulley joints and subsequently proposes a design methodology to synthesize a pair of variable radius pulleys to improve joint torque capacity over a large workspace. Experimental results show that newly synthesized variable radius pulleys significantly improve position tracking performance in the enlarged workspace.**

I. INTRODUCTION

Introduced by McKibben, pneumatic muscle actuation was used in the late 1950s mainly for prosthetic and orthotic applications. Recently, pneumatic artificial muscles (PAMs) are gaining popularity in robotics as safe actuators for manipulators. Due to their high force/weight and force/volume ratios, PAMs are suitable actuators for light weight designs. In addition, PAMs' output impedance is low over a wide frequency range as a result of its natural compliance and low inertia. These properties enable PAMs to reduce large impact forces to safe levels during unforseen collisions [8].

PAMs are simple in design, which consist of an inflatable rubber inner tube covered with a braided shell. When pressurized, the muscle shortens and generates a force axially. The magnitude of this force depends on both the muscle length and the applied pressure [1], [11]. Pneumatic muscle, by itself can only produce unilateral pulling forces. In order to produce bidirectional torque and thus span the whole range of motion, further design considerations are required. Drawing from biological principles of the human musculoskeletal structure, a pair of PAMs can be connected antagonistically via a pulley to generate bidirectional torque. The torque produced is a result of difference in applied muscle forces on each side of the pulley. An interesting feature of this design is the adjustable passive stiffness achieved by co-contraction [13].

PAMs-based antagonistic actuation comes with limitations in control bandwidth due to its natural compliance. To address the low bandwidth, Shin et al. proposed a hybrid actuation approach which consists of a pair of PAMs coupled to a low-inertia DC-motor in parallel [8] (Fig. 1). The low-pass behavior of PAMs naturally partitions the reference input torques between low frequency (macro) and high frequency (mini) actuation components. The macro torque component is primarily sustained by the muscles while the resultant torque error is compensated by the DC motor. This configuration improves the overall bandwidth as the fast DC motor compensates for the slow dynamics of the muscles.

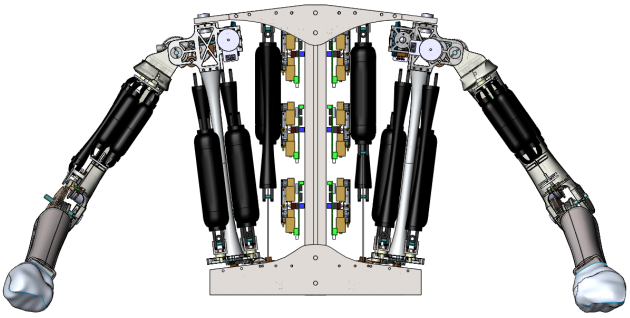

Fig. 1. Stanford Human-Friendly Robot with variable radius pulleys [10].

In addition to low bandwidth, PAMs-based joint suffers from restricted torque capacity and joint motion due to the limited contraction ratio of the muscles [9]. Typically, torque capacity can be increased by utilizing a larger pulley. However, a larger pulley radius decreases the workspace rapidly while producing only minimal improvement in torque capacity. In applications that require high torque over a large workspace, this trade-off is undesirable. Moreover, since joint properties like passive stiffness, workspace, and torque capacity are all dependent on the pulley radius and the highly nonlinear force-length relationship of the muscles, the task of selecting a pulley radius that meets specific application needs is not trivial.

Several methods have been proposed in literature to kinematically adjust spring force/torque using a variable radius pulley. Okada proposed a mechanism with non-circular pulleys and springs for an inner pipe inspection robot to generate uniform contact forces on pipe surfaces [5]. Endo et al. and Ulrich et al. employed non-circular pulleys and linear springs to achieve passive gravity compensation [3], [12]. In [4],

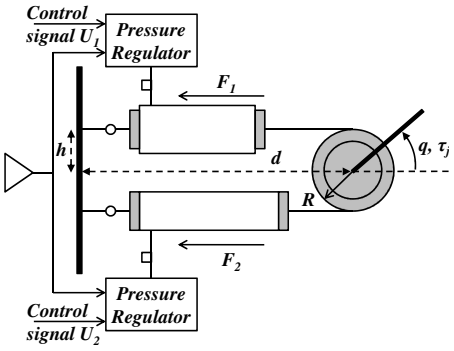

Fig. 2. Antagonistically driven air muscle joint [6].

a numerical algorithm was proposed to synthesize a pulley profile that improves the output torque of a shape memory alloy actuator.

In this paper, we modify the algorithm from [4] for PAMs and propose a design methodology to synthesize a pair of variable radius pulleys that maintains high torque capacity while satisfying passive stiffness and workspace requirements. The structure of the paper is as follows. Section II provides an analysis on the workspace, minimum available torque, and maximum achievable passive stiffness of a circular pulley joint. Limitations of circular pulley joints are also discussed. Subsequently, a design methodology to derive a pair of variable radius pulleys to meet workspace, stiffness, and torque capacity requirements is developed in Section III. Finally, section IV provides an application of the design methodology and a performance comparison between both pulleys. This paper concludes with a summary and some discussions on future research directions.

II. CIRCULAR PULLEY IN ANTAGONISTIC ACTUATION

A. Antagonistic Actuation

A typical PAMs-based antagonistic actuation system consists of a pair of air muscles, each connected to its own pressure regulator as shown in Fig. 2. Muscle forces are converted to torque via a pulley rigidly attached to the driven link. To control these forces, control signals are sent to the pneumatic valves to vary the internal pressures of the muscles. When pressure increases, the muscle expands radially and shortens in length to generate an axial contraction force.

Torque control is implemented by closing an outer loop around the force control loop. Given a pair of muscle forces, the output torque for a circular pulley joint, τ_j, is

$$\tau_j = R(F_1 - F_2) \tag{1}$$

where R is the pulley radius, and F_1 and F_2 represent the pair of muscle forces. Using force feedback from load cells, the inner force control loop compensates for the force/length hysteresis, and thus increases the closed loop bandwidth [6]. Due to actuation redundancy, there are infinite sets of muscle forces that produce the same τ_j. Additional control objectives such as stiffness control can be integrated to distribute the muscle forces [13].

B. Muscle Model

In our analysis, the static air muscle model developed by C. P. Chou et al. is adopted [1].

$$F = \frac{Pb^2}{4\pi n^2}\left(\frac{3L^2}{b^2} - 1\right) \tag{2}$$

where F is the force generated by the muscle, P is the internal gauge pressure, and L is the muscle length. The terms, b and n, are muscle constants. They represent the thread length and the number of turns of the thread around the muscle respectively. Clearly, F depends on both P and L.

C. Workspace vs. Output Torque vs. Pulley Radius

For PAMs, muscle force is nonlinearly related to the muscle length and also depends on the internal pressure. Thus, the relationship between output torque and workspace for a given pulley radius is not trivial [9]. To investigate the workspace and torque properties of a circular pulley joint with respect to pulley radius, we simulated a simple 1-DOF system shown in Fig. 2.

A typical torque capacity profile for a circular pulley joint is illustrated in Fig. 3. The workspace is defined as the largest span of joint motion subjected to feasible muscle contraction ratio, and is denoted as $\{q_{min}, q_{max}\}$ in Fig. 3. At the extremes of the workspace, the minimum available torques, τ_{min}, for a circular pulley joint is limited. This can be explained by Equation (2). When the joint angle, q, increases beyond the origin, the upper muscle shortens while the lower muscle lengtens by the same length. As a result, the upper muscle needs to be highly pressurized in order to move the joint upwards. The same scenario happens when q goes below the origin.

Typically, in order to increase τ_{min}, a larger pulley can be utilized. However, since a larger pulley rapidly saturates the available muscle contraction, the overall range of motion decreases drastically. The trade-off is undesirable since a

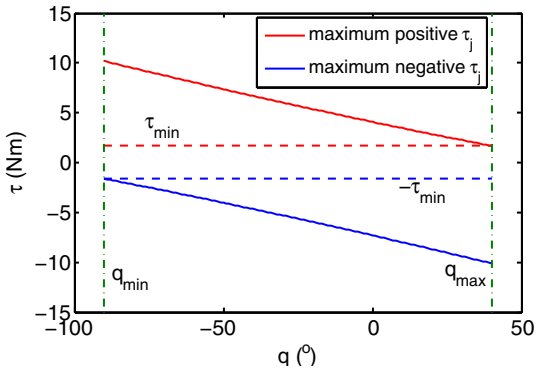

Fig. 3. Typical torque capacity profile of a circular pulley joint. Higher τ_{min} further limits range of motion, which is represented by the vertical green dashed lines.

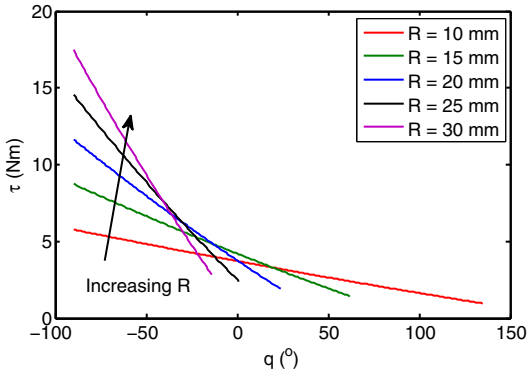

Fig. 4. Workspace vs. maximum positive torque of a circular pulley joint with respect to pulley radius. Increasing pulley radius results in improvement in torque capacity at the expense of large reduction in workspace.

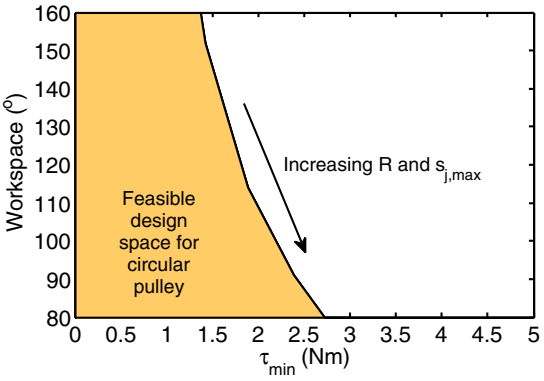

Fig. 5. Feasible design space for a circular pulley.

minimal increase in τ_{min} comes at the expense of a significant workspace reduction as shown in Fig 4. Therefore, a circular pulley joint is not able to produce high torques while maintaining a large workspace.

D. Passive Stiffness vs. Pulley Radius

The stiffness of a muscle, k, depends on both the change of force with respect to length and the internal air compressibility.

$$k = \frac{\partial P}{\partial L}\frac{b^2}{4\pi n^2}\left(\frac{3L^2}{b^2} - 1\right) + \frac{3PL}{2\pi n^2} \tag{3}$$

Assuming small pressure and volume changes at the operating point, $\frac{\partial P}{\partial L}$ can be neglected [2]. Combining with Equation (2), the stiffness of a PAM can be simplified as

$$k = \frac{6F}{(3L - \frac{b^2}{L})} \tag{4}$$

which is related to both the muscle's pressure and length. In an antagonistic configuration, the overall joint stiffness is obtained as

$$s_j = R^2(k_1 + k_2) \tag{5}$$

where k_i are the stiffness of each muscle $i \in \{1, 2\}$ as defined in (4). Thus, the range of achievable passive stiffness increases with pulley radius.

E. Limitations and Problem Statement

Fig. 5 summarizes how different joint properties vary with pulley radius. Given a specified workspace, the corresponding τ_{min}, maximum passive stiffness, $s_{j,max}$, and the required R can be determined within the feasible design space. Using a circular pulley, one is often unable to achieve an advantageous trade-off among workspace, τ_{min}, and s_j. When radius is increased, although a higher $s_{j,max}$ is achieved, the joint is unable to produce high τ_{min} while maintaining a large workspace. This is mainly a consequence of having just a single design variable, i.e., R in the joint design. To achieve a desired trade-off and thus a design that better suits application needs, a pair of variable radius pulleys can be employed for each of the muscles.

III. DESIGN METHODOLOGY

A. Overview

In this section, we give an overview in the design of a pair of variable radius pulleys to satisfy specifications of workspace and $s_{j,max}$ while achieving high τ_{min}. Although the pair of pulleys can be independently designed, a symmetrical configuration is employed where the pulley for the upper muscle is first designed, and subsequently adapted for the lower muscle. Such a configuration matches both positive and negative minimum available torques.

B. Torque Profile

When synthesizing the pulley for the upper muscle, we need to first design a desired torque capacity profile, $\tau_{1,Des}(q)$. It should be noted that any arbitrary profile cannot be employed. Since passive stiffness, s_j, is a parallel combination of stiffness components from each of the muscles, it can be expressed as

$$s_j = -\frac{\partial \tau_1}{\partial q} + \frac{\partial \tau_2}{\partial q} \tag{6}$$

where τ_1 and τ_2 are the torques generated by the upper and lower muscles, respectively. It is necessary for the upper muscle's desired torque profile to be a decreasing function with respect to q and for the lower muscle's profile to be an increasing function. Since we are employing a symmetrical configuration for the pulleys, it suffices to design a pulley for the upper muscle that satisfies the torque profile requirement.

A suitable candidate is a first order polynomial with negative gradient.

$$\tau_{1,Des}(q) = -mq + c \tag{7}$$
$$m \geq 0$$

This choice not only satisfies the requirements, but also yields a passive stiffness that is linearly dependent on the applied pressures, which will be explained in later sections.

C. Pulley Synthesis

To synthesize the pulley connected to the upper muscle that matches $\tau_{1,Des}(q)$, a numerical algorithm is utilized. This is based on [3] and [4] which was used for designing

joint torque profiles for a shape memory alloy actuator and a linear spring. We modified the algorithm in order to adapt it to PAMs-based system. The design procedure is as follows:

1) Set structural design parameters d, h in Figs. 2 and 6, as well as the initial arm angle, q_0, and desired torque profile, $\tau_{1,Des}(q)$, for the upper muscle.
2) Set muscle length as the maximum length, l_{max}, and the maximum internal pressure as P_{max}. The initial pulley radius is obtained as $r_0 = \tau_{1,Des}(q_0)/F_1$
3) Draw a tangent line to the circle, l_0, in order to intersect the attachment point of the muscle, P_0, in Fig. 6, where the center of the circle is O and its radius is r_0. Define C_0 as the intersection of l_0 and Y axis.
4) Draw a circle with radius of OP_0 and define points, $P_1, P_2, ..., P_n$, using a constant incremental angle, Δq. This is because kinematic inversion is used where the pulley centered at O is fixed while the attachment points of the muscle moves to unwind the pulley.
5) Choose a random point α on the tangent line, l_0. Obtain the muscle length, L_α, stretched between the segment, $\overline{\alpha P_1}$, and distance, r_α, of the straight line, αP_1, from the origin, O. The change of length of the muscle stretched from the point, α, is $(\overline{\alpha P_0} - \overline{\alpha P_1})$ because the flexible cable winding around the pulley is supposed to be non-ductile. Consequently, the muscle length is $l_\alpha = l_{max} - (\overline{\alpha P_0} - \overline{\alpha P_1})$, where the muscle force, $F_{1,\alpha}$, is computed from Equation (2) with $l = l_\alpha$.
6) Perform the operation in which the position of the point, α, is shifted until it agrees with the desired torque profile, $\tau_{1,Des}(q)$ using $F_{1,\alpha} \cdot r_\alpha$ by means of a convergent calculation such as Newton's method.
7) Make the position of the point, C_1, which is the first vertex of the pulley profile to be polygonally approximated.
8) Assume a new point, α, on the straight line, $\overline{C_1 P_1}$, and repeat the calculations of 5) through 7) for the points, α and P_2, to obtain C_2.
9) Repeat the above-mentioned procedure until the muscle length reaches the minimum contracted length, l_{min}. At this point the maximum range of motion is reached. Therefore, this range defines the overall workspace of the joint.

The series of contour vertices, $C_0, C_1, ..., C_n$, defines the profile of the pulley. To generate the second pulley, the pulley profile for the first pulley is rotated to the maximum joint angle in the achievable workspace found in 9). Subsequently, flip the pulley about the X axis. The initial length of the muscle for the second pulley is selected to be l_{min}.

D. Effects of m on Stiffness

Since the maximum pressure, P_{max}, is used in the pulley synthesis, the torque generated by muscles are

$$\tau_1 = \frac{P_1(-mq + c)}{P_{max}} \ , \ \tau_2 = \frac{P_2(mq + c')}{P_{max}} \qquad (8)$$

where τ_1, τ_2, P_1, and P_2 are generated torques and internal pressures of the upper and lower muscle, respectively. Using

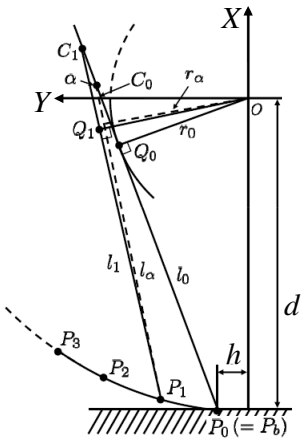

Fig. 6. Procedure for pulley synthesis [3].

Equation (6) and considering the stiffness contribution from the pair of symmetrical pulleys, the overall joint stiffness is derived as follows:

$$s_j = \frac{m(P_1 + P_2)}{P_{max}} \qquad (9)$$

The stiffness is linear to the applied pressures of both muscles, leading to a simpler stiffness model compared to that of a circular pulley where stiffness is related to pressure and muscle length.

E. Effects of m and c on Workspace and τ_{min}

We performed simulations on the design variables, m and c, of $\tau_{1,Des}(q)$ to understand how each of them affects workspace and torque capacity. The results are summarized graphically in Fig. 7

For a constant c, when m increases, the pulley profile converges from an elongated shape to a circular profile as shown in Fig. 8(a). Note that the elongated portion of the profile serves to enlarge the moment arm when the muscle contraction approaches saturation. As the profile converges to

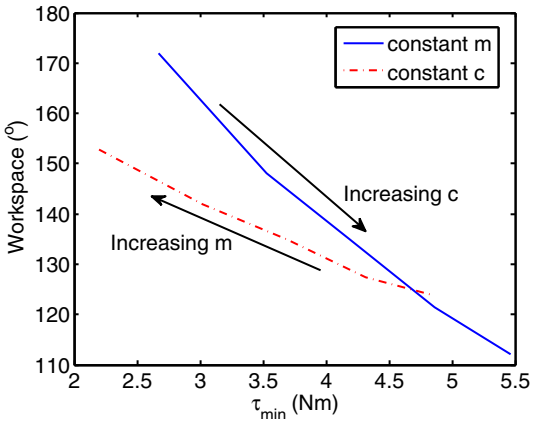

Fig. 7. Effects of m and c on workspace and τ_{min}. A blue solid line and a red dashed line show the effect of c given constant m = 1 and the effect of m given constant c = 8, respectively.

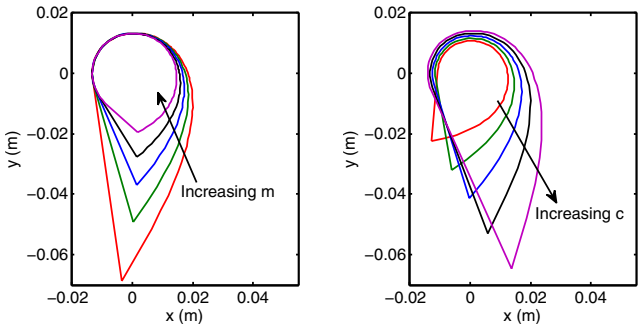

Fig. 8. Effects of m and c on pulley profile

a circular shape, the workspace increases since muscle length changes more slowly. However, the reduction of moment arm results in a lower τ_{min}.

When m is held constant while c increases, the pulley profile deviates from a circular shape to an elongated shape as shown in Fig. 8(b). As a result, muscle contraction saturates rapidly, and thus workspace reduces. However, with an increased moment arm, τ_{min} increases.

F. Design Procedure

A flowchart of the proposed design procedure is shown in Fig. 9. We first consider satisfying the stiffness requirement, which is often determined by robot safety and performance metrics [10]. Since stiffness is solely dependent on m, we can meet the desired stiffness with an appropriate choice of m. This leaves us with a problem of one design variable, i.e., c. By varying c, we are able to control the trade-off between workspace and τ_{min}.

IV. RESULTS AND DISCUSSIONS

A. Theoretical Comparison with Circular Pulley

The pair of variable radius pulleys offers additional design freedom and expands the workspace-τ_{min} design space. As illustrated in Fig. 10, designs employing a circular pulley results in a lower τ_{min} for the specified workspace when compared to joints with variable radius pulleys. When low

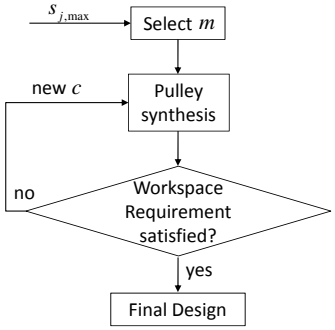

Fig. 9. Design procedure. Since stiffness is solely dependent on m, we first determine a stiffness by an appropriate choice of m. This leads to a problem of one variable. Subsequently, we vary only c to control the trade-off between workspace and τ_{min}.

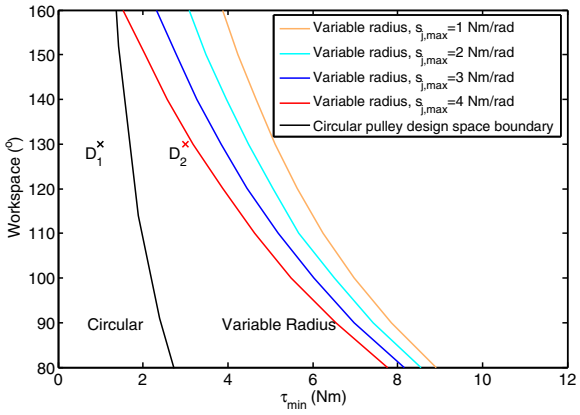

Fig. 10. Comparison of design spaces of both pulleys. When a higher torque is required (D_2), a variable pulley joint satisfies the desired workspace-torque characteristics unlike a circular pulley.

torque and large workspace designs are considered (D_1), both circular and variable pulley designs are suitable. However, when a higher torque is required (D_2), it is not feasible to design a circular pulley joint that satisfies the desired workspace-torque characteristics. However, using a pair of variable radius pulleys, we are able to meet the desired requirements.

B. Application of Design Methodology and Experiments

To validate the improved performance of a variable radius pulley joint over a circular pulley joint, we applied our design methodology to the elbow joint of a human-friendly robot. The required workspace is 145° with a maximum passive stiffness of 2.5 Nm/rad while the required minimum available torque over the entire workspace is 3 Nm. The synthesized pair of variable radius pulleys is shown in Fig. 11. The circular pulley joint fails to satisfy the desired torque capacity while the pair of variable pulleys satisfies all the requirements as shown in Table I. To experimentally validate the improved torque capacity, both pulleys were installed on a 1-DOF arm, which is driven by an antagonistic pair of PAMs, and position-stiffness control was performed. The PAMs are Shadow Robot's 20mm Air Muscles. The detailed characteristics are described in [7]. The joint was commanded to track a sinusoidal trajectory while regulating joint stiffness. At the extremes of the workspace, the limited

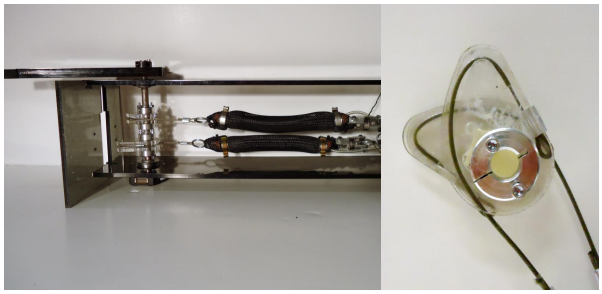

Fig. 11. 1-DOF testbed with variable radius pulleys. An antagonistic pair of PAMs drive the joint.

τ_{min} for circular pulley results in poor tracking performance as shown in Fig. 12.

TABLE I
PULLEY COMPARISON

	Design Goal	Circular Pulley (R=15.9mm)	Variable Radius Pulley (R=12.4 $\sim$ 30.2mm)
Workspace	$-90^\circ \sim 55^\circ$	$-90^\circ \sim 55^\circ$	$-90^\circ \sim 55^\circ$
τ_{min}	3 Nm	1.44 Nm	3.36 Nm

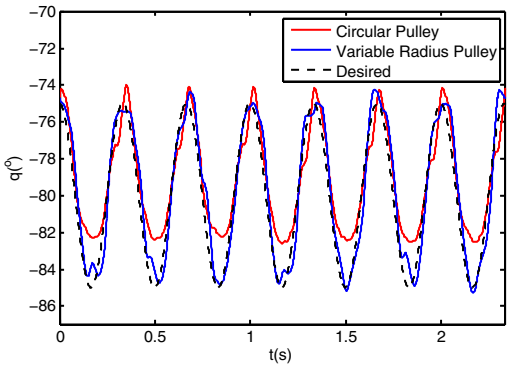

(a) Performance at -80°

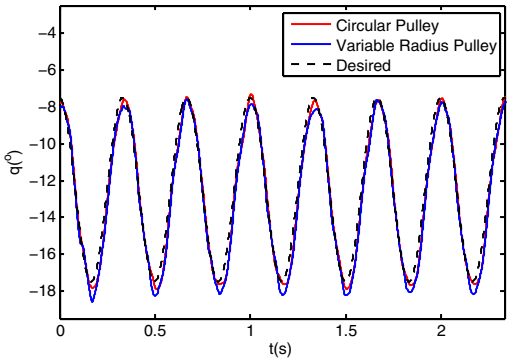

(b) Performance at -12.5°

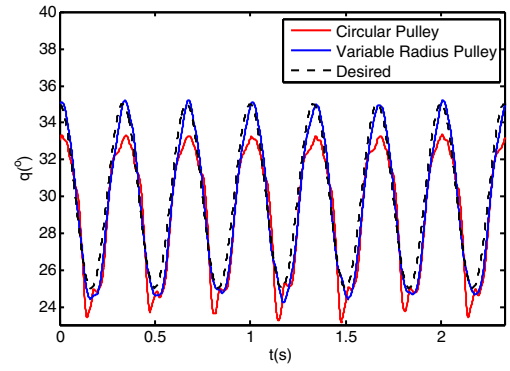

(c) Performance at 30°

Fig. 12. Tracking performance at different configurations. The joint was commanded to track a 3 Hz sinusoidal reference with joint stiffness regulated at 25% of the maximum stiffness. At the center of the workspace (-12.5°), the performance of both pulleys are comparable. However, at angles near to the ends of the workspace ($30^\circ, -80^\circ$), the limited torque capacity of the circular pulley joint results in significant roll-off.

V. CONCLUSIONS AND FUTURE WORK

We investigate the limitations of a conventional circular pulley joint in producing high torques while maintaining a large range of motion. Based on the analysis, we propose a methodology to design a pair of variable radius pulleys. The methodology expands the design space of a circular pulley joint, and thus yields designs that achieve higher torque capacity and larger workspace with desired stiffness. Furthermore, added torque capacity over the entire workspace enhances control performance particularly when either of the muscles is fairly stretched or contracted.

For future work, the newly designed pulleys will be integrated into the Stanford Human-Friendly Robot and advanced control strategies such as sliding mode control will be implemented to deal with the parametric uncertainties in the modeling of both muscles and variable radius pulleys. Additionally, performance and safety metrics will be also be used as control objectives in the stiffness control of the joint.

REFERENCES

[1] C. P. Chou, B. Hannaford, "Measurement and modeling of McKibben pneumatic artificial muscles", IEEE Transactions on Robotics and Automation, vol.12, no.1, pp.90-102, Feb 1996

[2] R. W. Colbrunn, G. M. Nelson, R. D. Quinn, "Modeling of braided pneumatic actuators for robotic control", Proceedings of the 2001 IEEE/RSJ International Conference on Intelligent Robots and Systems, vol.4, pp.1964-1970, 2001

[3] G. Endo, H. Yamada, A. Yajima, M. Ogata, S. Hirose, "A passive weight compensation mechanism with a non-circular pulley and a spring", Proceedings of the 2010 IEEE International Conference on Robotics and Automation, pp.3843-3848, 2010

[4] S. Hirose, K. Ikuta, K. Sato, "Development of Shape Memory Alloy Actuator. Improvement of Output Performance by the Introduction of a σ-Mechanism", Advanced Robotics, Vol.3, No.2, pp.89108, 1989.

[5] T. Okada, T. Kanade, "A Three-Wheeled Self-Adjusting Vehicle in a Pipe, FERRET-1", International Journal of Robotics Research, Vol.6, No.4, pp.6075, 1987

[6] I. Sardellitti, J. Park, D. Shin, O. Khatib, "Air muscle controller design in the distributed macro-mini (DM2) actuation approach", Proceedings of the 2007 IEEE/RSJ International Conference on Intelligent Robots and Systems, pp.1822-1827, 2007

[7] Shadow Robot Company Ltd., Http://www.shadowrobot.com

[8] D. Shin, I. Sardellitti, Y-L. Park, O. Khatib, M. Cutkosky, "Design and Control of a Bio-inspired Human-Friendly Robot", The International Journal of Robotics Research, vol.29, no.5, pp.571-584, 2010

[9] D. Shin, O. Khatib, M. Cutkosky, "Design methodologies of a hybrid actuation approach for a human-friendly robot", Proceedings of the 2009 IEEE International Conference on Robotics and Automation, pp.4369-4374, 2009

[10] D. Shin, F. Seitz, O. Khatib, M. Cutkosky, "Analysis of torque capacities in hybrid actuation for human-friendly robot design", Proceedings of the 2010 IEEE International Conference on Robotics and Automation, pp.799-804, 2010

[11] B. Tondu, P. Lopez, "Modeling and control of McKibben artificial muscle robot actuators", IEEE Control Systems Magazine, vol.20, no.2, pp.15-38, 2000

[12] N. Ulrich, V. Kumar, "Passive mechanical gravity compensation for robot manipulators"', Proceedings of the 1991 IEEE International Conference on Robotics and Automation, vol.2, pp.1536-1541, 1991

[13] G. Zong, R. Liu, "On the implementation of stiffness control on a manipulator using rubber actuators", Proceedings of the 1995 IEEE International Conference on Systems, Man and Cybernetics, vol.1, pp.183-188, 1995